DOI: 10.13009/EUCASS2017-582

DOI: ADD DOINUMBER HERE

Delayed detached eddy simulation of separated flows in a planar nozzle

E. Martelli†
Università della Campania Luigi Vanvitelli, via Roma 29, 81031, Aversa, Italy
emanuele.martelli@unicampania.it
P.P. Ciottoli, M. Bernardini, F. Nasuti, M. Valorani
Sapienza, University of Rome, via Eudossiana 18, 00184, Rome, Italy
pietropaolo.ciottoli@uniroma1.it, matteo.bernardini@uniroma1.it, francesco.nasuti@uniroma1.it, mauro.valorani@uniroma1.it
†Corresponding author

Abstract

The sea-level start-up of rocket engines is characterized by the nozzle overexpansion and an internal flow separation with a strong unsteady shock wave boundary layer interaction (SWBLI). This produces side-loads, which reduce the safe life of the engine. In this work, a 3D planar overexpanded nozzle has been simulated by means of the Detached Eddy Simulation technique. The pressure signals have been analyzed by the wavelet decomposition. The results indicate that the shock unsteadiness has been captured and that the characteristics frequencies are close to the ones available from literature. The shock excursion seems to be too high and requires further investigations.

1. Introduction

In nozzle supersonic flows, separation generates shock waves, which impinge on the walls. This shock wave boundary layer interaction (SWBLI) causes the shedding of vortical structures and the unsteadiness in the shock wave position. This produces dynamic side-loads, which reduce the safe life of the engine and can lead to the failure of nozzle structure.[15] According to Schmucker,[21] the origin of side-loads is due to an asymmetry of the separation location, which produces a tilted separation line and a momentum imbalance. A literature survey reporting the various studies on the side loads generation and separation shock configurations can be found in Hadjadj and Onofri[11] and in Reijasse et al.[20] But, in spite of all of these studies, a fundamental knowledge of supersonic flow physics in the presence of a shock separation interaction is still needed. Among the several tasks for necessary investigations recommended by Hadjadj and Onofri[11] one is related to the low frequency oscillations of a shock interacting with a turbulent flow separation. This phenomenon, consisting in fluctuating pressure loads and pulsating recirculating flows, should be carefully addressed by researchers and rocket nozzle designers. A lot of experimental work has been carried out to understand the unsteadiness of shocks in internal flows. Bogar et al.[2] investigated the unsteady flow characteristics of an overexpanded transonic diffuser. They observed that in the case of attached flow (or very mild separation), the characteristic frequencies have an acoustic nature, and scale with the distance of the shock from the diffuser exit. While, in the case of separated flows, the characteristic frequencies scale with the length of the inviscid core flow. Also Handa et al.[12] indicated two possible mechanisms for the shock oscillation. In one case, pressure disturbances, generated in the downstream turbulent separated region, force the shock to oscillate, resulting in a broad shape of the power spectral density. The other case foresees the reflection of a disturbance at the diffuser exit (acoustic feedback), resulting in a narrow-shaped power spectral density. Johnson and Papamoschou[13] have studied the unsteady shock behavior in an over-expanded planar nozzle. Their results indicate a low frequency piston-like shock motion without any resonant tones.

As far as large/detached eddy simulations (LES/DES) of this kind of flows are concerned, very few studies can be found in literature. Deck[3] carried out a delayed detached eddy simulation (DDES) of the end-effect regime in an axi-symmetric over-expanded rocket nozzle flow characterized by a restricted shock separation (RSS). While the experimentally measured main properties of the flow motion were rather well reproduced, the computed main frequency resulted to be higher than in the experiment. Olson and Lele[17] performed large eddy simulations of the experiments of Johnson and Papamoschou, finding an agreement between the experimental data and the computed frequency of the shock displacement. The origin of the unsteadiness was attributed to the confinement of exit area by the separated flow.

DOI: 10.13009/EUCASS2017-582

The use of a detached eddy simulation,[26] a hybrid RANS/LES method, allows to simulate the flows typically present in sub-scale cold flow supersonic nozzles,[3,14] which are characterized by Reynolds number of the order of one million and are still hardly predictable by means of large eddy simulation technique. In this work, the 3D planar nozzle described in the experiments of Johnson and Papamoschou[13] and simulated with the LES technique by Olson and Lele[17] has been reproduced by means of the DDES technique.[22] The first main target is the comparison between computational and experimental data regarding the unsteady flow behavior, to assess if the DDES technique is able to describe this kind of flow. The second main target is to address the issue of the significant delay of transition from RANS to LES in the supersonic shear layers that can be found in over-expanded nozzles. To overcome this issue, the enhanced versions of DES equipped with a new definition of the sub-grid length-scale[22] is adopted. Unlike the original definition attached to DES, i.e., simply the maximum local grid spacing, the new one depends, in addition to the grid spacing, also on the local vorticity vector. In addition, it includes a kinematic measure which serves as indicator of the nearly 2D grid-aligned flow regions which are typical of the initial region of separated shear layers. This brings about a significant reduction of the sub-grid viscosity in such regions and should unlocks the Kelvin-Helmholtz instability. The last task is the wavelet spectral analysis of the dynamic pressure signals. Wavelet transform is an analysis tool well suited to the study of multi-scale, non-stationary processes occurring over finite temporal domains.[27] In particular it is able to detect the localized variations of power within a time series. In fact, by decomposing a time series into time-frequency space, one is able to determine both the dominant modes of variability and how these modes vary in time.

2. Computational setup

To better understand the unsteadiness of SWBLI in supersonic nozzles and the role played in the generation of side loads, large eddy simulations should be ideally carried out to capture the larger structures of the turbulent flow. Presently, the computational cost of a wall-resolved LES is still unfordable for high-Reynolds number wall-bounded flows. Hybrid RANS/LES modeling approaches have been proposed to simulate massively separated flows, such as the well-known DES.[24] A general feature of this approach is that the whole attached boundary layer is treated resorting to RANS, while LES is applied only in the separated flow regions.

2.1 Physical model

The three-dimensional Navier-Stokes equations for a compressible, viscous, heat-conducting gas, which are adopted in this study, can be written as follows

$$\begin{aligned}\frac{\partial \rho}{\partial t}+\frac{\partial(\rho\, u_j)}{\partial x_j}&=0,\\ \frac{\partial(\rho\, u_i)}{\partial t}+\frac{\partial(\rho\, u_i u_j)}{\partial x_j}+\frac{\partial p}{\partial x_i}-\frac{\partial \tau_{ij}}{\partial x_j}&=0,\\ \frac{\partial(\rho\, E)}{\partial t}+\frac{\partial(\rho\, E u_j+p u_j)}{\partial x_j}-\frac{\partial(\tau_{ij}u_i-q_j)}{\partial x_j}&=0,\end{aligned}\tag{1}$$

where ρ is the density, u_i is the velocity component in the i-th coordinate direction ($i = 1, 2, 3$), E is the total energy per unit mass, p is the thermodynamic pressure. The total stress tensor τ_{ij} is the sum of the viscous and the Reynolds stress tensor,

$$\tau_{ij}=2\rho\,(\nu+\nu_t)\,S^*_{ij}\qquad S^*_{ij}=S_{ij}-\frac{1}{3}S_{kk}\,\delta_{ij},\tag{2}$$

where the Boussinesq hypothesis is applied through the introduction of the eddy viscosity ν_t, and where $S_{ij} = \left(u_{i,j}+u_{j,i}\right)/2$ is the strain-rate tensor, ν the molecular viscosity, depending on temperature T through Sutherland's law. Similarly, the total heat flux q_j is the sum of a molecular and a turbulent contribution

$$q_j=-\rho\,c_p\left(\frac{\nu}{\mathrm{Pr}}+\frac{\nu_t}{\mathrm{Pr}_t}\right)\frac{\partial T}{\partial x_j},\tag{3}$$

Pr, Pr_t being the molecular and turbulent Prandtl numbers, assumed to be 0.72 and 0.9, respectively. Hybrid RANS/LES capabilities are provided through the implementation of the delayed detached-eddy simulation (DDES) approach based on the Spalart-Allmaras (SA) model,[25] which involves a transport equation for a pseudo eddy viscosity $\tilde{\nu}$

$$\frac{\partial(\rho\tilde{\nu})}{\partial t}+\frac{\partial(\rho\,\tilde{\nu}\,u_j)}{\partial x_j}=c_{b1}\tilde{S}\rho\tilde{\nu}+\frac{1}{\sigma}\left[\frac{\partial}{\partial x_j}\left[(\rho\nu+\rho\tilde{\nu})\frac{\partial\tilde{\nu}}{\partial x_j}\right]+c_{b2}\,\rho\left(\frac{\partial\tilde{\nu}}{\partial x_j}\right)^2\right]-c_{w1}f_w\rho\left(\frac{\tilde{\nu}}{\tilde{d}}\right)^2,\tag{4}$$

DOI: 10.13009/EUCASS2017-582

where $\tilde{d}$ is the model length scale, f_w is a near-wall damping function, $\tilde{S}$ a modified vorticity magnitude, and $\sigma, c_{b1}, c_{b2}, c_{w1}$ model constants. The eddy viscosity in Eq. 2 is related to $\tilde{\nu}$ through $\nu_t = \tilde{\nu} f_{v1}$, where f_{v1} is a correction function designed to guarantee the correct boundary-layer behavior in the near-wall region. In DDES the destruction term in Eq. 4 is designed so that the model reduces to pure RANS in attached boundary layers and to a LES sub-grid scale one in the detached flow regions. This is accomplished by defining the length scale $\tilde{d}$ as

$$\tilde{d} = d_w - f_d \max(0, d_w - C_{DES}\,\Delta), \tag{5}$$

where d_w is the distance from the closest wall, Δ is the subgrid length-scale, controlling the wavelengths resolved in LES mode. C_{DES} is a calibration constant equal to 0.65. The function f_d, designed to be 0 in boundary layers and 1 in LES regions, reads as

$$f_d = 1 - \tanh\left[(10 r_d)^3\right], \qquad r_d = \frac{\tilde{\nu}}{k^2\, d_w^2\, \sqrt{U_{i,j}U_{i,j}}}, \tag{6}$$

where $U_{i,j}$ is the velocity gradient and k the von Karman constant. The introduction of f_d distinguishes DDES from the original DES approach[26] (usually denoted as DES97), ensuring that boundary layers are treated in RANS mode also in the presence of "ambiguous" grids in the sense defined by Spalart et al.,[25] for which the wall-parallel spacings do not exceed the boundary layer thickness. It must be noted that in the original paper[25] the coefficient multiplying r_d in the expression for f_d is equal to 8. This number comes from a calibration done simulating a zero-pressure-gradient flat plate. A coefficient equal to 10 seems to be more useful in a flow with a pressure gradient. The DDES strategy prevents the phenomenon of model stress depletion, consisting in the excessive reduction of the eddy viscosity in the region of switch (grey area) between RANS and LES, which in turn leads to grid-induced separation. Unlike in the original DDES formulation, the sub-grid length scale in this work is not defined as the largest spacing in all coordinate directions $\Delta_{\max} = \max(\Delta x, \Delta y, \Delta z)$, but it depends on the flow itself, through f_d as follows

$$\Delta = \frac{1}{2}\left[\left(1 + \frac{f_d - f_{d0}}{|f_d - f_{d0}|}\right)\Delta_{\max} + \left(1 - \frac{f_d - f_{d0}}{|f_d - f_{d0}|}\right)\Delta_\omega\right], \tag{7}$$

where $f_{d0} = 0.999$ (in the original paper[4] it is equal to 0.8), Δ_ω is a characteristic length scale, which takes in to account the orientation of the vorticity and it has been introduced by Deck et al.[4] It is defined as

$$\Delta_\omega = \sqrt{N_x^2 \Delta x \Delta z + N_y^2 \Delta z \Delta x + N_z^2 \Delta x \Delta y} \tag{8}$$

where $N = \frac{\omega}{||\omega||}$ is the unit vector, which gives the orientation of the vorticity ω. In the early stages of a shear layer of spanwise direction in z, equation [8] gives $\Delta_\omega = \sqrt{\Delta x \Delta y}$. In such a way Δz, which is usually greater than the others, is excluded from the computation of the length scale. This definition should prevent a delayed development of instabilities in the shear layer and, consequently, a late transition of the flow to a full turbulent condition. In addition, following Shur et al.,[22] another modification to the characteristics length scale should be made to promote an important decrease of the sub grid scale (SGS) viscosity in the initial part of the shear layer. A kinematic measure is necessary to identify the almost 2D flow areas, which could require a nearly implicit LES (ILES) method, to accelerate the triggering of the Kelvin-Helmotz instability. Such a measure has been defined as Vortex Tilting Measure (VTM) and has the following expression

$$\mathrm{VTM} = \frac{\sqrt{6}|(\mathbf{S}\cdot\omega)\times\omega|}{\omega^2\sqrt{3tr(\mathbf{S^2}) - [tr(\mathbf{S})]^2}} \tag{9}$$

where $\mathbf{S}$ is the strain tensor and $tr(\cdot)$ means trace. This measure will be close to zero in the quasi 2D region, where the vorticity is an eigenvector of the strain tensor, and close to one in the fully turbulent zones, since the lack of a strong correlation between the strain eigenvectors and vorticity. Now, the definition of the length scale reads as

$$\Delta_{\omega,VTM} = \Delta_\omega \cdot F_{KH}(< VTM >) \tag{10}$$

where F_{KH} is the function aimed at unlocking the instabilities:

$$F_{KH}(< VTM >) = \max\{F_{KH}^{\min}, \min\{F_{KH}^{\max}, F_{KH}^{\min} + \frac{F_{KH}^{\max} - F_{KH}^{\min}}{a_2 - a_1}(< VTM > -1)\}\} \tag{11}$$

The angle brackets indicate averaging of VTM over the neighboring cells, in order to smooth this kinematic measure. $F_{KH}^{\max} = 1.0$, $F_{KH}^{\min} = 0.1$, a_1=0.15 and $a_2 = 0.3$. Finally, it is necessary that $F_{KH}(< VTM >)$ is equal to 1 in inviscid regions, in order to avoid numerical issues. The result of equation [9] is multiplied by $\max\{1, 0.2\nu/\nu_t\}$.

DOI: 10.13009/EUCASS2017-582

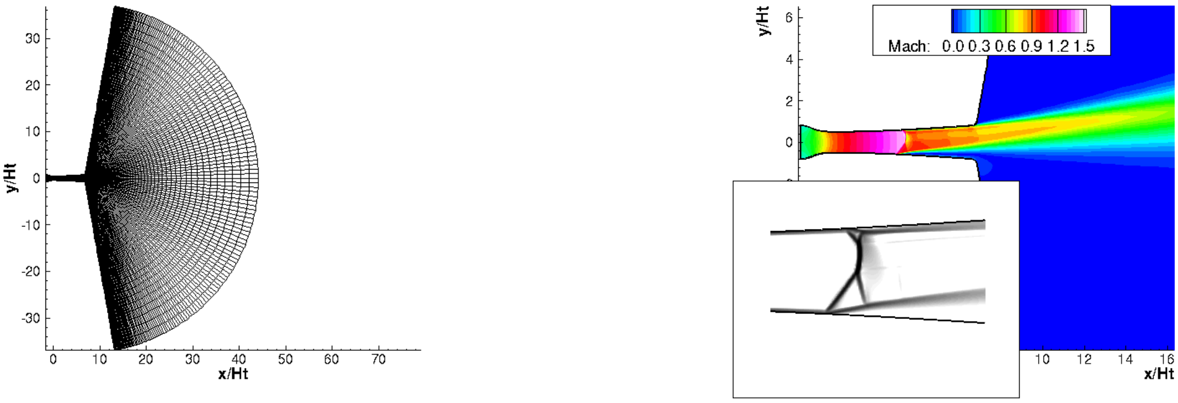

(a)

(b)

Figure 1: a) Computational domain and mesh; b) Rans Mach number flow field and enlargement of the shock.

2.2 Numerical method

Numerical simulations are carried out by means of a in-house, fully validated compressible flow solver, that exploits a centered second-order finite volume approach and takes advantage of an energy consistent formulation (away from shocks). Cell-face values of the flow variables are obtained from the cell-centered values through suitable reconstructions. In smooth flow regions, the reconstruction is carried out in such a way that the overall kinetic energy of the fluid is preserved, in the limit of inviscid, incompressible flow.[18] This property is particularly beneficial for flow regions treated in LES mode, where the grid is sufficiently fine to support the development of LES content, and where the only relevant dissipation (in addition to the molecular one) should be that provided by the turbulence model. The discretization scheme is made to switch to third-order weighted essentially-non-oscillatory (WENO) near discontinuities, as controlled by a modified Ducros sensor.[8] The gradients normal to the cell faces needed for the viscous fluxes, are evaluated through second-order central-difference approximations, obtaining compact stencils and avoiding numerical odd-even decoupling phenomena. Time advancement of the semi-discretized system of ODEs resulting from the spatial discretization is carried out by means of a low-storage third-order Runge-Kutta algorithm.[1] The code is written in Fortran 90, it uses domain decomposition and it fully exploits the message passing interface (MPI) paradigm for the parallelism.

3. Test case description

A two-dimensional schematic of the computational domain adopted for the simulation is presented in figure 1(a). It includes the nozzle and the external ambient. The nozzle geometry has been taken from case 3 of the work of Johnson et al.[13] The throat height is equal to 17.8 mm, the nozzle length (from the throat) is equal to 117 mm, the width is equal to 63.5 mm. The area ratio A_e/A_t is equal to 1.7. A Cartesian structured mesh is generated using the conformal mapping algorithm of Driscoll and Vavasis[6] and the open-source tool gridgen-c. The computational mesh consists of $N_x \cdot N_y \cdot N_z = 512 \cdot 256 \cdot 96$ cells for a total number of $N_{xyz} \approx 12.6 \cdot 10^6$ cells. The grid density of this test case is very similar to the mesh "B" of Olson and Lele.[17] In the inlet station a subsonic flow is prescribed by imposing total pressure, total temperature and the flow direction. At the exit section a characteristics based boundary conditions prescribing the back pressure are assigned. In order to avoid any acoustic coupling a sponge is imposed from $x/H_t = 30$ to the end of the domain at $x/H_t = 43$. The top and bottom surfaces are treated as adiabatic no-slip walls. In the spanwise direction the extent of the domain is $L_z/H_t = 0.9$ and periodic boundary conditions are applied, as in the work of Olson and Lele.[17] The 3D DES initial condition is obtained from an extrusion in the spanwise direction of the 2D steady state RANS solution. To promote the development of turbulent structures, a sinusoidal perturbation in the spanwise direction with maximum magnitude of 0.5% has been superimposed on the density field. The simulations were performed on the supercomputers Galileo (IBM NextScale) and Marconi (Lenovo NeXtScale Platform) of the Italian Computing Center CINECA. The computational time step is equal to $1.3 \cdot 10^{-5}$s and the simulation ran approximately for 0.06 s, after an initial transient period of 0.02 s (approximately 10 low-frequency cycles of the shock motion) that was discarded. The maximum CFL number is 0.5.

The present internal flowfield is characterized by the nozzle pressure ratio $NPR = p_0/p_a$, where p_0 and p_a denote

DOI: 10.13009/EUCASS2017-582

the chamber and ambient pressure respectively. In this work the NPR selected is 1.7 (p_0= 1.7 bar), equal to the case 3 of the study of Olson and Lele.[17] The nozzle Reynolds number is based on the chamber values and the throat half height:

$$Re = \frac{\sqrt{\gamma}}{\mu}\frac{p_0 H_t/2}{\sqrt{R_{air}T_0}} = 3.3 \cdot 10^5,$$

where γ is the constant specific heat ratio, μ is the molecular viscosity evaluated at the chamber temperature T_0= 300 K and R_{air} is the air gas constant.

4. Discussion of the results

The main characteristics of the instantaneous flowfield are shown in figure 2. The 3D turbulent structures are represented by showing a positive iso-value of the Q-criterion.[7] This qualitative criterion identifies tube-like vortical structures as the regions where the second invariant of the velocity gradient tensor Q is positive:

$$Q = \frac{1}{2}(\Omega_{ij}\Omega_{ij} - S_{ij}S_{ij}) > 0$$

where S_{ij} and Ω_{ij} are the symmetric and anti-symmetric components of ∇u. The iso-surface are colored by the local value of the streamwise velocity. The slice in the last Z planes show the field of the magnitude of the density gradient, useful to individuate the shocks and the shear layers. Looking at the bottom wall, which develops the most important separated region, it is possible to notice at first the roll-up of almost two-dimensional vortical structures in the shear layer, which are then replaced by three-dimensional structures developing downstream. It can be seen from the picture that there is still an important region, just downstream the flow separation, which remains in the so called gray area: in this zone the flow is not treated in RANS mode nor in LES mode. So, it seems that the VTM is not sufficient to trigger the instabilities in such a case. It could be necessary to investigate if a lower value of the C_{DES} constant, as proposed by Spalart,[23] and/or a finer mesh could improve the simulation. The top wall, characterized by a very small separation, remains almost in RANS mode and develops a turbulent content just at the nozzle exit. A global unsteadiness with fluctuations in the separation shock position characterizes the flowfield, as shown in figure 3, where different snapshots of the density gradient field, showing the various position reached by the shock system, are reported during half a cycle. The non-dimensional time is indicated as $\tau = tU_p/H_t$, where t is the dimensional time and U_p is the quasi 1D velocity at the nozzle exit, computed by the isentropic relations and the nozzle area ratio.

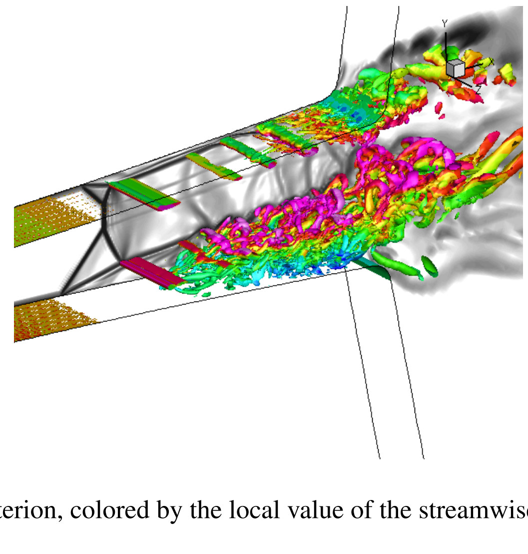

Figure 2: Iso-surface of the Q-criterion, colored by the local value of the streamwise velocity. The slice in the Z-plane shows the field of $||\nabla\rho||$.

4.1 Wall pressure signature

The statistical properties of the fluctuating wall pressure are analyzed by evaluating the standard deviation. Figure 4a) shows a set of instantaneous, spanwise averaged wall pressure distributions and illustrates the entity of the shock excursion. The standard deviation of the bottom wall pressure fluctuations (σ_w/p_0), obtained by averaging over the homogeneous spanwise direction and time, is reported in figure 4b). Within the attached boundary layer σ_w is zero, since,

DOI: 10.13009/EUCASS2017-582

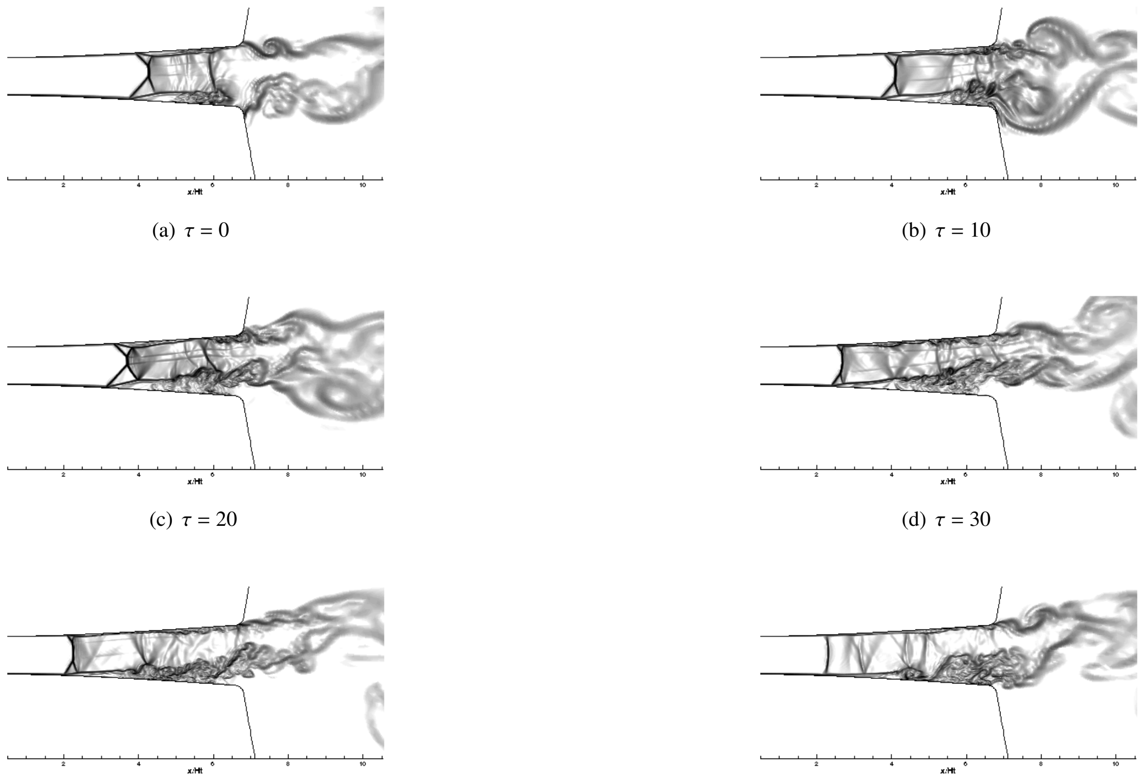

(a) $\tau = 0$ (b) $\tau = 10$ (c) $\tau = 20$ (d) $\tau = 30$ (e) $\tau = 40$ (f) $\tau = 50$

Figure 3: Numerical Schlieren at different time instants during half a cycle.

according to the DDES approach, this flowfield region is automatically treated in RANS mode. Instead, downstream of the separation point, there is a peak in the standard deviation value, corresponding to the excursion zone of the shock system. Moving downstream, the first part of the recirculation region is characterized by a decrease of σ_w, while a mild increase is observable in the last part of the nozzle. It can be noted that the distribution of the wall pressure fluctuations is qualitatively very similar to the distributions found in other classical shock wave/boundary layer interaction; see for example the experimental findings of Dupont on an incident shock on a flat plate[9, 19] and of Dolling on a supersonic flow over a compression ramp.[5] In figure 4b) the position of two numerical pressure probes are also reported. P_1 is located where the wall pressure fluctuation standard deviation has the maximum value corresponding to the shock oscillation, while P_2 is located in the turbulent recirculation region. Figure 5 shows a temporal slot of the wall pressure signals from probes P_1 and P_2. It can be seen that the first signal is characterized by the passage of the foot of the separation shock. When the shock is downstream the probe P_1, the wall pressure value is related to the attached supersonic flow, while when the shock is upstream the probe, the wall pressure value is related to the recirculating subsonic region. The probe P_2 is most of the time downstream the shock, therefore the signal is typical of a turbulent separated region. The downward spikes in the pressure behavior indicates that sometime the shock approaches probe P_2.

4.2 Wavelet spectral analysis

The continuous wavelet transform is applied to the unsteady wall pressure signals in order to decompose them in the time-frequency space. An extended review of the application of wavelets to study turbulence phenomena can be found in Farge,[10] while only the key theoretical aspects are here reported. The continuous wavelet transform of a discrete time sequence p_n, with equal spacing δt and $n = 0 \ldots N-1$, is defined as the convolution of p_n with a scaled and translated version of the mother wavelet ψ_0:

$$W_n(s) = \sum_{n'=0}^{N-1} p_n \cdot \psi^* \left[\frac{(n'-n)\delta t}{s} \right] \tag{12}$$

where $*$ denotes the complex conjugate. By varying the wavelet scale s and translating along the time index n, one can construct a picture showing both the amplitude of any features versus the scale and how this amplitude varies with

DOI: 10.13009/EUCASS2017-582

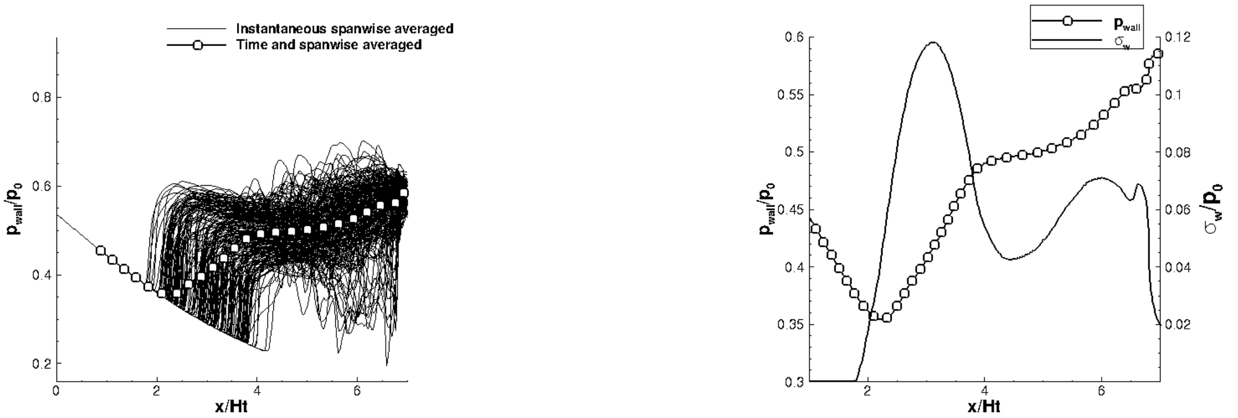

(a) (b)

Figure 4: a) Streamwise distributions of instantaneous spanwise averaged wall pressures and of time and spanwise averaged wall pressure; b): streamwise distributions of time and spanwise averaged wall pressure and of pressure fluctuations standard deviation σ_w/p_0.

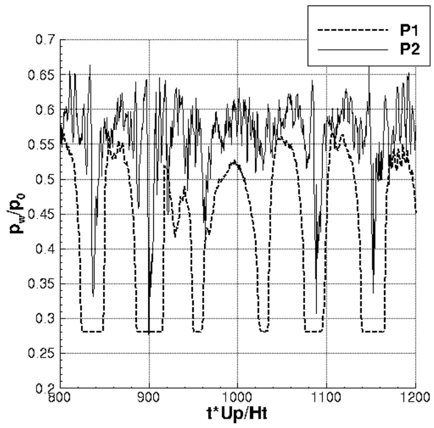

Figure 5: Temporal slot of the wall pressure signals from probes P_1 and P_2

time. In this study, the Morlet wavelet has been chosen since higher resolution in frequency can be achieved when compared with other mother functions. It consists of a plane wave modulated by a Gaussian:

$$\psi_0(\eta) = \pi^{-1/4} e^{i\omega_0\eta} e^{-\eta^2/2} \tag{13}$$

where η is a non dimensional time parameter and ω_0 is the non dimensional frequency, here taken equal to 6 to satisfy the admissibility condition.[27] This wavelet is shown in figure 6 both in the time and frequency domains. The relationship between the equivalent Fourier period λ and the wavelet scale s can be found analytically.[27] For the Morlet wavelet with $\omega_0 = 6$ it is possible to find that $\lambda = 1.03s$. From the definition of the wavelet coefficient one can directly define the wavelet power spectrum (WPS) as $|W_n(s)|^2$. The WPS allow to build the wavelet scalogram, which provides a decomposition of the energy onto the scale-time (or frequency-time) plane. A Fourier-like spectrum can be simply recovered by a time averaging (marginal wavelet power spectrum).

Figure 7a) shows the wavelet power spectrum of the wall pressure signal from probe P_1. The wavelet decomposition indicates that most of the energy is located in an almost uniform way around a Strouhal number, $S_t = fH_t/U_p$ where f is the frequency, equal to 0.017. Occasionally, bursts at higher energy appear. These peaks due to the bursts indicate the influence of intermittency on the shock motion. The WPS of the signal from P_2 is reported in figure 7b). The effect of the shock motion on the spectrum is always present, with most of the energy concentrated around S_t=0.017. In addition, the energy coming from the turbulent structures is also present at higher S_t. The WPS is now characterized by an increased degree of intermittency: burst of high energy are followed by region of low energy and they are spread over a wider region of S_t, between 0.03 and 0.3. The marginal WPS's of the two pressure signals are shown in figure 8.

DOI: 10.13009/EUCASS2017-582

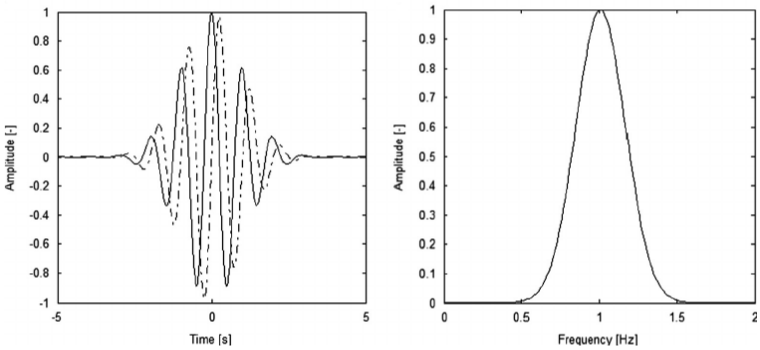

Figure 6: Morlet Wavelet base. Left: real part (solid line) and imaginary part (dashed line) in the time domain; right: the corresponding wavelet in the frequency domain.

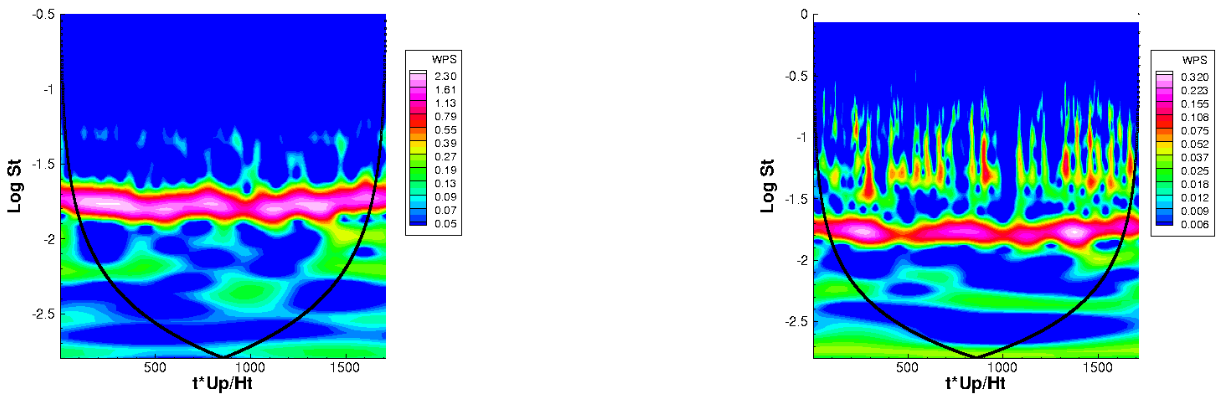

(a)

(b)

Figure 7: a) Wavelet Power Spectrum of the pressure signal at P1; b) Wavelet Power Spectrum of the pressure signal at P2

DOI: 10.13009/EUCASS2017-582

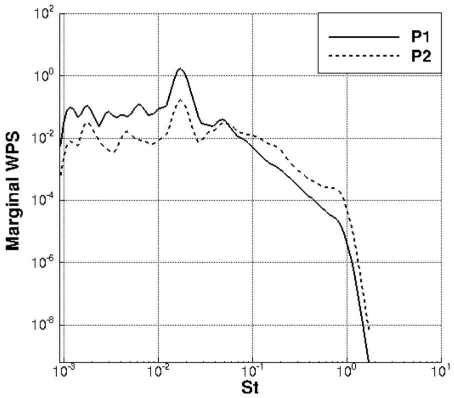

Figure 8: Marginal wavelet power spectrum of the wall pressure signals from probes P_1 and P_2.

This plot can give an information similar to that given by the Fourier spectrum. Both the spectrum from P_1 and P_2 are characterized by the peak around S_t = 0.017, due to the shock movement. The signal from P_1 is characterized by an higher energy, since it is located in the middle of the shock oscillation. The spectrum from P_2 shows an higher energy from S_t greater than 0.06. This energy is characteristic of the fully turbulent subsonic recirculating region. The values

Table 1: Comparison between DES, LES[17] and experiment[13]

	DDES	LES	Exp.
Shock Strouhal	0.017	0.0122	$0.01 \leq S_t \leq 0.1$
Shock excursion	2.4 H_t	1.4 H_t	0.9 H_t

of the shock excursion length and of the peak shock S_t number are compared with the results of a LES[17] of the same test case and of the experiment[16] in table 1. It can be seen that the computed peak S_t number is in the range of the experimental values and close to the LES value. However, it is observed that the shock excursion length is higher than the LES value and much higher than the experimental value. Further investigation are therfore necessary in order to investigate this discrepancy between DES, LES and the experiment.

5. Conclusions

A delayed detached eddy simulation of a planar nozzle with flow separation has been carried out and the results have been compared with experimental results and LES results taken from literature. The nozzle flow simulated in this study is characterized by a strong non-symmetric separation shock with a classical lambda shape and by an important recirculation zone. The simulation is able to capture a self-sustained unsteadiness of the shock system. A classical statistical description of this unsteadiness has been carried out. The shock region is characterized by a well defined peak in the wall pressure fluctuations standard deviation distribution. The spectral analysis has been conducted by using the Morlet wavelet transform, which is a well suited tool to analyze non stationary time series. According to the wavelet decomposition, the shock movement is characterized by a concentration of energy around a S_t number equal to 0.017. Bursts of higher energy are also presents in this region, indicating an effect of the turbulence intermittency. The peak S_t is close to the LES and the experimental values. The wavelet power spectrum in the recirculating region is always influenced by the shock movement at S_t = 0.017. But it also shows the effect of the fully development of turbulence. In fact, for S_t greater than 0.06 , the spectrum is characterized by a collection of alternating high and low energy events. The excursion length of the shock is too high compared to the LES and experimental values. The DES model needs therefore a deep assessment. In the next steps, the effect of the C_{DES} constant, of the grid density and of the computational domain will be faced.

6. Acknowledgments

M. Bernardini was supported by Scientific Independence of young Researchers (SIR) program 2014 (Active Control Of shock wave/ Boundary layer Interactions (jACOBI) project, grant RBSI14TKWU), which is funded by the

DOI: 10.13009/EUCASS2017-582

Ministero Istruzione Università e Ricerca. The simulations have been performed thanks to computational resources provided by the Cineca Italian Computing Center under the Italian Super Computing Resource Allocation initiative (grant $Iscra\ C/DESROCK$ and $Iscra\ B/jACOBI$). Wavelet software was provided by C. Torrence and G. Compo. The authors would like to acknowledge S. Pirozzoli, who developed the baseline Fortran flow solver.

References

[1] M Bernardini and S Pirozzoli. A general strategy for the optimization of runge–kutta schemes for wave propagation phenomena. *J. Comput. Phys.*, 228:4182–4199, 2009.

[2] T. J. Bogar, M. Sajben, and J. C. Kroutil. Characteristic Frequency and Lenght Scales in Transonic Diffuser Flow Oscillations. (81–1291), 1981. AIAA 14th Fluid and Plasma Dynamics Conference.

[3] Sébastien Deck. Delayed detached eddy simulation of the end-effect regime and side-loads in an overexpanded nozzle flow. *Shock Waves*, 19(3):239–249, 2009.

[4] Sébastien Deck. Recent improvements in the Zonal Detached Eddy Simulation (ZDES) formulation. *Theoretical and Computational Fluid Dynamics*, 26(6):523–550, 2012.

[5] D. S. Dolling and C. T. Or. Unsteadiness of the shock wave structure in attached and separated compression ramp flows. *Experiments in Fluids*, 3(1):24–32, 1985.

[6] Tobin A. Driscoll and Stephen A. Vavasis. Numerical Conformal Mapping Using Cross-Ratios and Delaunay Triangulation. *SIAM Journal on Scientific Computing*, 19(6):1783, 1998.

[7] Yves Dubief and Franck Delcayre. On coherent-vortex identification in turbulence. *Journal of Turbulence*, 1:1–22, 2000.

[8] F. Ducros, V. Ferrand, F. Nicoud, D. Darracq, C. Gacherieu, and T. Poinsot. Large-eddy simulation of the shock/turbulence interaction. *J. Comput. Phys.*, 152:517ˇ2013549, 1999.

[9] P. Dupont, C. Haddad, and J. F. Debiève. Space and time organization in a shock-induced separated boundary layer. *Journal of Fluid Mechanics*, 559:255, 2006.

[10] M. Farge. Wavelet Transforms and Their Applications to Turbulence. *Annu. Rev. Fluid Mech.*, 24:395–457, 1992.

[11] A. Hadjadj and M. Onofri. Nozzle flow separation. *Shock Waves*, 19:163–169, 2009.

[12] Taro Handa, Mitsuharu Masuda, and Kazuyasu Matsuo. Mechanism of Shock Wave Oscillation in Transonic Diffusers. *AIAA Journal*, 41(1):64–70, 2003.

[13] Andrew D. Johnson and Dimitri Papamoschou. Instability of shock-induced nozzle flow separation. *Physics of Fluids*, 22(1):1–13, 2010.

[14] E Martelli, Pietro P. Ciottoli, M Bernardini, F Nasuti, and M Valorani. Mechanism of Shock Wave Oscillation in Transonic Diffusers. *AIAA Journal*. accepted for publication.

[15] L.H. Nave and G.A. Coffey. Sea level side loads in high-area-ratio rocket engines . *Propulsion Conference; 9th; Nov. 5-7, 1973; Las Vegas, NV; US*, 1973.

[16] B. Olson and S. Lele. Large-Eddy Simulation of an over-expanded planar nozzle . *41st AIAA Fluid Dynamics Conference*, (June), 2011.

[17] Britton J. Olson and Sanjiva K. Lele. A mechanism for unsteady separation in over-expanded nozzle flow. *Physics of Fluids*, 25(11):110809, 2013.

[18] S. Pirozzoli. Numerical methods for high-speed flows. *Annu. Rev. Fluid Mech.*, 43:163–194, 2011.

[19] S. Pirozzoli and M. Bernardini. Direct numerical simulation database for impinging shock wave/turbulent boundary-layer interaction. *AIAA Journal*, 49(6):1307–1312, 2011.

[20] P. Reijasse, S. Palerm, and B. Pouffary. Side loads and thermal loads in rocket nozzles. Overview of the CNES-ONERA ATAC programme. *Int. J. Eng. Syst.Model. Simul.*, 3:87ˇ201398, 2011.

DOI: 10.13009/EUCASS2017-582

[21] R.H. Schmucker. Flow process in overexpanded chemical rocket nozzles, part 2: Side loads due to asymmetric separation. *NASA TM-77395*, 1984.

[22] Mikhail L. Shur, Philippe R. Spalart, Mikhail Kh. Strelets, and Andrey K. Travin. An enhanced version of des with rapid transition from rans to les in separated flows. *Flow, Turbulence and Combustion*, 95(4):709–737, 2015.

[23] Philipe R. Spalart and Langley Research Center. *Young-person's guide to detached-eddy simulation grids [microform] / Philippe R. Spalart*. National Aeronautics and Space Administration, Langley Research Center ; Available from NASA Center for Aerospace Information Hampton, Va. : Hanover, MD, 2001.

[24] Philippe R. Spalart. Detached-Eddy Simulation. *Annual Review of Fluid Mechanics*, 41(1):181–202, 2009.

[25] P.R. Spalart, S. Deck, M.L. Shur, K.D. Squires, M.Kh. Strelets, and A.K. Travin. A new version of detached-eddy simulation, resistant to ambiguous grid densities. *Theor. Comput. Fluid Dyn.*, 20:181–195, 2006.

[26] P.R. Spalart, W.H. Jou, M. Strelets, and S.R. Allmaras. Comments on the feasibility of les for wings, and on a hybrid rans/les approach. In *Advances in DNS/LES*, pages 137–147. Greyedn Press, 1997.

[27] Christopher Torrence and Gilbert P Compo. A Practical Guide to Wavelet Analysis. *Bulletin of the American Meteorological Society*, 79(1):61–78, 1998.